

# Dalton Transactions

Accepted Manuscript



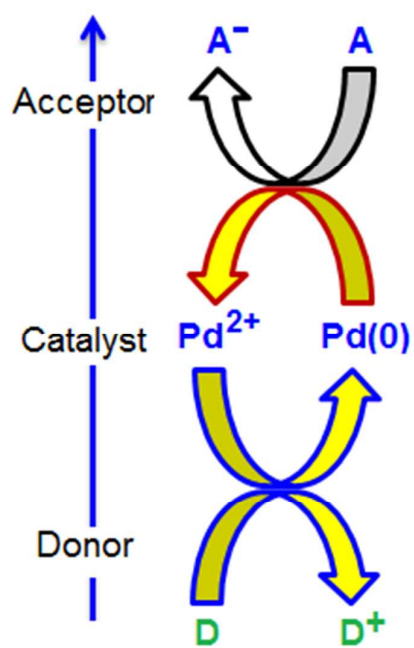
This is an *Accepted Manuscript*, which has been through the Royal Society of Chemistry peer review process and has been accepted for publication.

*Accepted Manuscripts* are published online shortly after acceptance, before technical editing, formatting and proof reading. Using this free service, authors can make their results available to the community, in citable form, before we publish the edited article. We will replace this *Accepted Manuscript* with the edited and formatted *Advance Article* as soon as it is available.

You can find more information about *Accepted Manuscripts* in the [Information for Authors](#).

Please note that technical editing may introduce minor changes to the text and/or graphics, which may alter content. The journal's standard [Terms & Conditions](#) and the [Ethical guidelines](#) still apply. In no event shall the Royal Society of Chemistry be held responsible for any errors or omissions in this *Accepted Manuscript* or any consequences arising from the use of any information it contains.

## Table of Content:



Catalytic activity of palladium nanoparticles for PCET reaction.

## ***In-situ* generation of a high-performance Pd-polypyrrole composite with multi-functional catalytic properties**

**Meenakshi Choudhary,<sup>a</sup> Rafique Ul Islam,<sup>a</sup> Michael J Witcomb,<sup>b</sup> Kaushik Mallick<sup>a\*</sup>**

<sup>a</sup>Department of Chemistry, University of Johannesburg, P.O. Box 524, Auckland Park 2006, South Africa.

<sup>b</sup>DST/NRF Centre of Excellence in Strong Materials, University of the Witwatersrand, Private Bag 3, WITS 2050, South Africa.

\*Corresponding author: E-mail: *kaushikm@uj.ac.za*

We report on a bottom up approach for the synthesis of a Pd-polypyrrole nanocomposite material. The composite material was characterized by means of different techniques, such as UV-vis, IR, and Raman spectroscopies, which offered information about the chemical structure of the polymer, whereas electron microscopy images provided information regarding the morphology of the composite material and the distribution of the metal particles in the polymer matrix. During the synthesis of the nanocomposite, the Pd nanoparticles act as a catalyst for a model proton-coupled electron transfer reaction. The Pd-polypyrrole nanocomposite material was also used as a catalyst for the electro-catalytic detection of tryptophan, a precursor for some neurotransmitters.

### **1. Introduction**

Metal nanoparticles are of significant interest as they show exceptional electronic, optical, and catalytic properties due to their quantum size effects. Nanoparticles are currently under intensive study for applications in optical [1] and electronic devices [2], sensors [3], biomedical applications [4] and as catalysts in different types of chemical reactions [5]. The main challenge in the application of these materials is agglomeration and that can be overcome through particle stabilization. Polymer stabilized metal nanoparticles have attracted much attention recently as a new research direction in catalysis [6–8]. The polymer matrices serve both as the support as well as the stabilizer of the nanoparticles thus providing a mechanism to prevent particle agglomeration. Palladium based catalysts, in particular nanoscale palladium particles, have recently drawn enormous attention due to their versatile role in organic synthesis [9–11]. The use of palladium nanoparticles in catalysis is not only industrially important [12–14], but also is scientifically interesting since they provide details of the mechanism of the reactions.

In the present investigation, we synthesized polypyrrole encapsulated palladium nanoparticles using an *in-situ* polymerization and composite formation (IPCF) method. IPCF is a facile synthesis technique carried out under ambient temperature conditions during which the Pd-acetate acts as an oxidizing agent that facilitates the oxidative polymerization of pyrrole while, on the other hand, the reduction of metal salt produces metal nanoparticles. During the polymerization process, the reduction of 4-nitrophenolate and methylene blue supports the catalytic effect of a proton-coupled electron transfers reaction. The Pd-polypyrrole nanocomposite material was used also as an electrocatalyst to investigate the electrochemical recognition of tryptophan by a cyclic voltammetry (CV) technique.

## 2. Experimental section

### 2.1. Materials

Pyrrole, ammonium persulfate (APS), potassium tetrachloro-palladate ( $K_2PdCl_4$ ), 4-nitrophenol, methylene blue (MB),  $K_4Fe(CN)_6 \cdot 3H_2O$  and tryptophan were purchased from Sigma-Aldrich of analytical purity and used without further purification. Toluene was obtained from Merck, and ultra-pure water (specific resistivity  $> 17M\Omega cm$ ) was used in this experiment wherever required.

### 2.2. Procedure

4-nitrophenolate (4NP) was made by adding sodium hydroxide to a water solution of 4-nitrophenol to secure a final concentration of  $10^{-4} \text{ mol dm}^{-3}$ . Similarly, methylene blue solution was made by adding ultra-pure water to obtain a final concentration of  $10^{-4} \text{ mol dm}^{-3}$ . Water solutions of APS and  $K_2PdCl_4$  were made by adding ultra-pure water to obtain a final concentration of  $10^{-2} \text{ mol dm}^{-3}$ .

### 2.3. Experimental details

(a) In a typical experiment, 0.030 g of pyrrole was diluted in methanol (15 mL) in a conical flask, after which 10 mL of  $K_2PdCl_4$  ( $10^{-2} \text{ mol dm}^{-3}$ ) was added slowly to it. A colloidal solution appeared at the bottom of the flask. The solution was allowed then to stand at rest for half an hour. Subsequently, TEM and SEM specimens were prepared by pipetting 2  $\mu L$  of the deposited material onto lacey, carbon coated, copper grids and allowed to air dry. A small portion of the product was used for optical characterization, the remaining fraction being dried under vacuum for 30 mins for the XRD and XPS analyses.

(b) In the first set of catalytic experiments, 1.5 mL of 4NP ( $10^{-4} \text{ mol dm}^{-3}$ ) was mixed with 60  $\mu L$  of pyrrole ( $10^{-2} \text{ mol dm}^{-3}$ ) in two quartz cuvettes. To the above solutions, 60  $\mu L$  APS

( $10^{-2}$  mol dm $^{-3}$ ) was added in one cuvette and 60  $\mu$ L K $_2$ PdCl $_4$  ( $10^{-2}$  mol dm $^{-3}$ ) was added to the other cuvette.

(c) In the second set of experiments, 1.5 mL MB was mixed with 0.5 mL of pyrrole (1.0 mol dm $^{-3}$ ) in two quartz cuvettes. To the above solutions, 0.5 mL APS ( $10^{-3}$  mol dm $^{-3}$ ) was added in one cuvette and 0.5 mL K $_2$ PdCl $_4$  ( $10^{-3}$  mol dm $^{-3}$ ) was added to the other cuvette. The progress of the reactions was monitored using a spectrophotometer.

## 2.4. Characterization

Transmission electron microscopy (TEM) was performed at an accelerating voltage of 197 kV in a Philips CM200 transmission electron microscope equipped with a LaB $_6$  source. An ultrathin window energy-dispersive X-ray system (EDX) and a Gatan Imaging Filter (GIF) attached to the TEM were used to determine the chemical composition of the samples. SEM studies were performed in a TESCAM VEGAS operating at 2–10 kV. To prevent possible charging, the samples were sputter coated with a thin uniform layer of carbon before viewing. The UV-vis spectra were measured using a Shimadzu UV-1800 UV-VIS spectrophotometer with a quartz cuvette. IR spectra were collected utilizing a Shimadzu IRAffinity-1 with a resolution of 0.5 cm $^{-1}$ . Raman spectra were acquired using the green (514.5 nm) line of an argon ion laser as the excitation source. Light dispersion was undertaken via the single spectrograph stage of a Jobin–Yvon T64000 Raman spectrometer. The X-ray diffraction (XRD) patterns were recorded on a Shimadzu XD-3A X-ray diffractometer operating at 20 kV using Cu-K $\alpha$  radiation ( $k = 0.1542$  nm). The measurements were performed over a diffraction angle range of  $2\theta = 20^\circ$  to  $70^\circ$ . The XPS spectra were collected in an ultra-high-vacuum chamber attached to a Physical Electronics PHI 560 ESCA/SAM system. Electrochemical measurements were carried out with a mini Autolab PGSTAT 910 potentiostat connected to a computer. A three-electrode system was used in the experiment with a bare electrode and a modified Glossy Carbon Electrode (GCE) as the working electrode. Ag/AgCl electrode (saturated KCl) and a Pt wire electrode were used as the reference and counter electrodes respectively. The catalyst was deposited on the working electrode using a ‘drop and dry’ method. After each run, the electrode was washed and an identical amount of new catalyst was applied as a coating to the electrode for the next study.

## 3. Results and discussion

The SEM image (Fig. 1A) shows the chain-like morphology of the product consisting of spherical units. The average diameter of a unit was about 100 nm while the chains are a few

micrometres in length. The TEM image (Fig. 1B) shows the uneven surface on the spheres. The higher magnification TEM images (Fig. 1C and D) show a high density distribution of dark spots. Such images and the stereo images (not shown) clearly indicate that the 2–4 nm diameter nanoparticles are encapsulated and homogeneously distributed within and throughout the product matrix. The EDX analysis (Fig. 2A) obtained from the electron beam being focused onto a dark spot confirms that these spots are palladium. Focusing the beam between the dark spots yielded no X-ray peaks for palladium. To identify the chemical state of the palladium, X-ray photoelectron spectroscopy (XPS) measurements were carried out. The Pd 3d region of the XPS spectrum of the Pd-polypyrrole composite is illustrated in Fig. 2B, which reveals the presence of Pd 3d<sub>5/2</sub> and 3d<sub>3/2</sub> peaks at binding energies of 335.35 and 340.60 eV respectively. These binding energy values are in accordance with those reported for metallic palladium [15]. XPS analysis also confirmed that 1.93 wt% Pd was present on the surface of the polypyrrole matrix. The crystalline nature of the palladium nanoparticles was confirmed by electron diffraction on single nanoparticles (not shown) and from XRD measurements (Fig. 2C). The strong (111) Bragg reflection indicates that the Pd-particles possess a highly oriented, face-selective, crystalline character.

The optical behaviour of the product was studied by Raman and FT-IR spectra analysis. Fig. 3A shows the Raman spectra of resultant material prepared by pyrrole and Pd-acetate using an *in-situ* approach. Two sharp peaks at 1540 and 1589 cm<sup>-1</sup> are attributed to the C=C ring stretching and N–H in-plane bending vibrations. A small peak at 1487 cm<sup>-1</sup> can be assigned to N–C stretch vibration. The vibrational peak at 1364 cm<sup>-1</sup> is due to both C–C and C=C stretching. A shoulder-like appearance at 1390 cm<sup>-1</sup> result from the N–C ring stretching mode [16], while the characteristic vibration band at 1248 cm<sup>-1</sup> is assigned to a ring deformation mode. The position of the inter-plane C–H bending and stretching modes is clearly evident at 1155 and 1210 cm<sup>-1</sup> respectively [16, 17].

Fig. 3B, spectra (a), shows a typical FT-IR spectrum of the product obtained during the reaction between pyrrole and Pd-acetate. The bands above 2500 cm<sup>-1</sup> are responsible for the aromatic C–H and N–H stretching vibrations. The prominent band observed above 1700 cm<sup>-1</sup> corresponds to formation of a carbonyl group, which is due to the over-oxidized structure of the polypyrrole [18–20]. The band occurring at 1469 and 1415 cm<sup>-1</sup> are for the C–N stretching vibration in the ring. The polypyrrole ring breathing vibration is located in the region 1250 to 1100 cm<sup>-1</sup>. The peak at 1111 cm<sup>-1</sup> is attributed to the breathing vibration of the pyrrole ring [21]. The bands of C–H and N–H in-plane deformation vibration are located

at  $1021\text{ cm}^{-1}$  while the band at  $744\text{ cm}^{-1}$  corresponds to C–H out-of-plane bending vibration [22]. The bands above  $2500\text{ cm}^{-1}$  (Fig. 3B) are responsible for the aromatic C–H and N–H stretching vibrations. The spectroscopic evidence confirms the formation of polypyrrole. For a comparison, we also synthesized polypyrrole using pyrrole and APS as a precursor and the oxidizing agent respectively. The product had a similar FTIR spectrum, Fig. 3B, spectra (b), that we recorded during the reaction between pyrrole and Pd-acetate. From reference to the optical properties and microscopic images, it can be confirmed that a Pd-polypyrrole nanocomposite was produced during the reaction between pyrrole and Pd-acetate.

### 3.1. Recognition of biomolecules using Pd-polypyrrole as an electrocatalyst

Development of rapid and sensitive methods for the detection of biomolecules is important for both clinical and numerous non-clinical applications. tryptophan, 2-amino-3-(1H-indol-3-yl)-propionic acid, is an essential amino acid and a precursor for serotonin, melatonin and niacin [23]. It has been implicated as a possible cause of schizophrenia and early diagnosis is very important for the proper treatment of the patient. It has been reported that spectroscopy, chemiluminescence, electrophoresis, chromatography and electro-analysis methods have been used for tryptophan determination [24]. Among these methods, electrochemical techniques have received considerable attention for the detection of biomolecules due to their sensitivity, simplicity and low cost. However, the electrochemical detection of tryptophan at unmodified electrode surfaces is not ideal due to sluggish electron transfer processes and the high over-potential for the oxidation of tryptophan [25]. Much effort has been devoted to finding new materials to modify electrodes in order to reduce the over-potential of tryptophan. Various modified electrodes have been applied to the determination of the tryptophan concentration in pharmaceutical and clinical samples utilizing nafion [26], butyryl-choline [27], carbon nanotubes [28], 1-[4-ferrocenyl ethynyl] phenyl]-1-ethanone [29] and a carbon nanotube-cobalt salophen complex [30] with detection limits of 1.6 nM,  $6.0\times 10^{-7}\text{ M}$ ,  $2.0\times 10^{-8}\text{ M}$ ,  $1.8\times 10^{-6}\text{ M}$  and  $1.0\times 10^{-7}\text{ M}$  of tryptophan respectively.

Functional nanomaterials with unique physical and chemical properties have provided significant advantages for biological detection. Metallic nanoparticles are interesting materials with respect to their unique electronic and electrocatalytic properties which depend on their size and morphology [31, 32]. The efficiency of the electronic and electrochemical redox properties makes these classes of nanostructured materials very promising for technological applications. Metal nanoparticles have also been used as a modifier of

electrodes for tryptophan analysis. Silver nanoparticles and a rutin complex film modified graphite electrode have been reported for tryptophan determination [33]. Gold nanoparticles have been much explored as components for biosensors development due to the capability to increase the electronic signal when a biological component is maintained in contact with the nanostructured surface. On the other hand, silver, platinum, palladium, copper, cobalt and other metals have been extensively explored in biosensor development [34–38]. Palladium is one of the preferred metals used as an electro-catalyst and different methodologies have been attempted to incorporate Pd particles into polymer matrices for fabrication of Pd modified electrodes [36, 39].

In the present work, we have compared the affinity and sensitivity of polypyrrole and Pd-polypyrrole for the electrochemical detection of tryptophan. Cyclic voltammetry (CV) of electroactive species of  $[\text{Fe}(\text{CN})_6]^{3-/4-}$  (FCN) has been used widely to test the barrier kinetics of the interface. The extent of kinetic hindrance to the electron transfer process increases with increasing film thickness and decreases with the defect density of the barrier. Fig. 4A shows the CV responses of 0.5 mM of FCN at bare GCE (a), the polypyrrole modified GCE (b), and a Pd-polypyrrole modified GCE (c) at pH 7.5, operating at a scan rate of  $50 \text{ mVs}^{-1}$ . After modifying the electrode with polypyrrole, a decrease in the redox peak current was observed (curve b), indicating that the polypyrrole acts as an electron and mass transfer blocking layer and thus hinders the diffusion of ferricyanide toward the electrode surface. In contrast, for the Pd-polypyrrole modified electrode, the voltammetric response of ferricyanide (curve c) is restored close to that obtained at the bare GCE (curve a). This demonstrates that the Pd nanoparticles have been successfully assembled on the electrode surface and provide the necessary conduction pathways, while also acting as nanoscale electrodes in promoting the electron transfer between the analyte (ferricyanide) and the electrode surface. The decreasing peak height indicates the passivation of the electrode surface.

Fig. 4B shows the cyclic voltammogram of bare GCE (a) in the absence, and (b) in the presence of the analyte (0.2mM tryptophan) in 0.01mM phosphate buffer at pH 7.5, utilizing a scan rate of  $50 \text{ mVs}^{-1}$ . The figure reveals an enhanced peak current of about  $\sim 2.0 \mu\text{A}$  in the presence of tryptophan when only the bare GCE was used as the working electrode. A noticeable current response change was observed when the electrode was modified with polypyrrole in the absence and in the presence of tryptophan. In Fig. 4B, curve (c) is the voltammogram of polypyrrole modified GCE in the absence of tryptophan. A broad area with an anodic peak position at about 1.15V results from the oxidative response of polypyrrole

whereas, in the presence of 0.2mM tryptophan, Fig. 4B, curve (d), the anodic peak position appears at a lower potential region resulting from the oxidation of tryptophan at 0.89V.

Comparing the cyclic voltammogram of the polypyrrole modified electrode in the absence of tryptophan (Fig. 4B, curve (c)) with that of the Pd-polypyrrole modified electrode also in the absence of tryptophan (Fig. 5, curve (a)) reveals similar curves with the exception of  $\sim 3.0 \mu\text{A}$  enhancement of the anodic peak current for the latter electrode over the former. This implies that the presence of Pd nanoparticles has improved the charge transfer at the interface.

The CV response of the Pd-polypyrrole modified electrode in the presence of tryptophan (0.20 mM) (Fig. 5, curve (b)) showed a well separated anodic peak at 0.75V with a current value of  $28 \mu\text{A}$ . Increasing the concentration of tryptophan to 0.40 and 0.60 mM (Fig. 5, curves (c) and (d) respectively) resulted in an increasing current while maintaining the same anodic peak position. The results demonstrated the key role played by the Pd-nanoparticles on the electrocatalytic oxidation of tryptophan.

### 3.2. Mechanism of formation of the Pd-polypyrrole composite

Among conducting polymers, polypyrrole and its derivatives are of particular interest owing to their high conductivity, stability in the oxidized state and interesting redox properties. The simplicity of the synthetic procedures and availability of the initial monomers are also attractive features of polypyrrole. A wide variety of methods have been applied to the preparation of polypyrrole by the oxidative polymerization of their monomer [40]. Chemical synthesis of polypyrrole has a long history. Polypyrrole has been prepared by the oxidation of the monomer (pyrrole) using ammonium persulfate (APS) [41], aqueous or anhydrous  $\text{FeCl}_3$  [42, 43] as well as other salts of iron (III) and copper (II) [44, 45] as chemical oxidants. In the present work, Pd-acetate was used as the oxidant for the synthesis of polypyrrole. Oxidative polymerisation of pyrrole to polypyrrole proceeds via the oxidation of pyrrole to a radical cation, which subsequently couples with another radical cation to form bipyrrrole. This process is then repeated to form longer chains. Each step of the polymerization is associated with the release of an electron ( $e^-$ ) and a proton ( $\text{H}^+$ ) (Scheme 1). The released electron is then used to reduce the Pd ion to form a Pd atom [46]. Subsequently, coalescence of the atoms results in the formation of clusters which stabilize within the polymer.

### 3.3. Pd nanoparticles as a catalyst for a proton coupled electron transfer reaction

The electron-transfer step is important in many homogeneous and heterogeneous reactions [47, 48]. Electron transfer in association with proton transfer is a well-known mechanism in chemistry, biology as well as in catalysis. The interest for proton-coupled electron transfer (PCET) reactions results from the fact that they play a key role in all the processes leading to energy storage into chemical bonds and thus for all expected renewable energy systems based on solar fuels [49]. Heterogeneous excited-state PCET is potentially important for systems involving solar energy conversion [50]. TiO<sub>2</sub> and other high-band gap semiconductor-based dye-sensitized photo-electro-synthesis cells are driven by photo-excitation and electron injection by bound chromophores or by a direct-band-gap excitation process [50]. A combined electrochemical and theoretical study has suggested that hydrogen production from weak acids catalyzed by NiFe hydrogenases involves a proton-coupled electron transfer step [51]. A mononuclear ruthenium complex has shown a multiple proton-coupled electron transfer [52] towards multi-electron transfer reactions which are known to be active catalysts for water oxidation. The cobalt-porphyrin system has been utilized as a catalyst for a hydrogen evolution reaction followed by an electron transfer (ET) and proton transfer (PT) pathway mechanism from carboxylic acid [53]. Oxidation of phenols is an extremely important reaction in many areas of natural and artificial chemistry in which electron transfer is inevitably associated with proton transfers. A mechanistic analysis has confirmed that the catalytic oxidation of phenols follows a concerted PCET pathway [54]. Oxidation reactions of alcohols with the Ru(IV)-oxo complexes proceed via a concerted proton-coupled electron transfer mechanism [55]. In the electron transfer step, there may be a redox potential difference between the donor and the acceptor, which may restrict or slow down the passage of an electron. An effective catalyst with an intermediate redox potential value between the donor-acceptor partners helps the electron transfer and acts as an electron relay system. Metal nanoparticles are well-known examples of this type of redox catalyst.

Fig. 6A shows the UV-vis spectra of 4NP in the presence of pyrrole and APS at different time intervals. From the figure, it can be seen that an incomplete quenching of the absorbance spectra of 4NP at 400 nm, peak (a), took some 204 min. As mentioned earlier, polymerization of pyrrole is an oxidation process and in the presence of an oxidizing agent (APS), it forms a radical cation with the release of an electron (e<sup>-</sup>) and a proton (H<sup>+</sup>). The gradual quenching of the 4NP spectra indicates the reduction of the nitro group. The emergence of the peak at about 320 nm, peak (b), is due to the formation of the polymer. The reduction mechanism of

4NP involves a single electron transfer (SET) mechanism with the formation of a radical cation followed by protonation (Scheme 2). The electrons and protons which are generated during the polymerization reaction participate in the reduction process of 4NP, an example of the proton coupled electron transfer reaction. Fig. 6B, curve (a), is the UV-vis spectra of 4NP, and in the presence of pyrrole and  $K_2PdCl_4$ , a complete quenching of the absorbance peak of 4NP occurred in about 2 min. In this reaction, the palladium (II) salt acts as an oxidizing agent, like other metal salts [45], that polymerizes pyrrole to form polypyrrole. The released electrons during the process of polymerization play a dual role in: (i) the formation of a radical-cation on the nitrogen of the nitro group (first step of the nitro-group reduction mechanism, Scheme 2) and (ii) reduce the  $K_2PdCl_4$  to form catalytically active palladium nanoparticles [56]. The *in-situ* generated Pd particles then catalyze the reduction of 4NP. Decreasing the concentration of 4NP, as indicated by the UV-vis spectrum at 400 nm, Fig. 6A, a new absorption peak developed at 320 nm, which results from the  $\pi^*-\pi$  transition and is due to the formation of polypyrrole [57]. The intensity of the absorption peak increases, as marked by an upward direction arrow, indicating the increase of polypyrrole concentration with time. When  $K_2PdCl_4$  was used as the oxidant, the absorption peak of 4NP (Fig. 6B) completely quenched and a new absorption band appeared at 320 nm again resulting from the formation of polypyrrole [57]. A shoulder-like feature at around 420 nm corresponds to the bipolaron transition, which is a feature of the oxidized state of polypyrrole. A similar kind of phenomenon also happens in the reduction process of MB, which involves the receiving of two electrons associated with two protons (Scheme 3). Fig. 7A, curve (a), and 7B, curve (a), show the UV-vis spectrum of MB with an absorption intensity peak at 665 nm. After the addition of pyrrole and APS, the absorbance value decreased due to a dilution effect as shown in Fig. 7A, curve (b). Initially, a rapid quenching of the dye was observed, but the rate of reaction was drastically retarded within a short period of time, there being no significant reduction after an hour. Similarly, Fig. 7B, curve (b), is the UV-vis spectrum of MB immediately after the addition of pyrrole and  $K_2PdCl_4$ . Within 2 mins of the addition, there was no characteristic peak for MB. The spectrum, Fig. 7B, curve (c), is due to the formation of Pd-polypyrrole composite. For a comparison, the UV-vis spectrophotometric property of the blank samples of polypyrrole (a) and Pd-polypyrrole (b) in absence of 4NP and MB respectively (Fig. 8) were studied and the spectral features corroborated with the above statements. In both spectra, the absorption band in the range of 300 to 350 nm corresponded to the formation of polypyrrole. Both the shoulder-like appearance observed from 415 to 500

nm (indicated by an arrow, Fig. 8, spectrum a) and a broad absorption band starting from 450 nm to around 750 nm seen in Fig. 8, spectrum (b), can be assigned to the bipolaron transition of the polymer. The position of this absorption band depends on various factors such as counter ions, solvent, chemical structure and the morphology of the polymer [58].

PCET reactions are those in which an electron and a proton are transferred together [59]. The particularity of such reactions is that the electron and the proton are transferred to different centres [60, 61]. Sequential transfer of electron and proton pathways is lower in energy than concerted pathways [59]. The multiple site electron-proton transfer reaction is another class of the PCET reaction in which (a) an 'electron-proton donor' transfers 'electrons and protons' to spatially separated acceptors or (b), an 'electron-proton acceptor' accepts 'electrons and protons' from spatially separated donors [59]. In the present work, we have coupled two reaction systems in which the pyrrole polymerization process releases both an electron plus a proton, and the reduction of the 4NP (or MB) occurs through it receiving an electron and a proton, an example of a 'proton coupled electron transfer' reaction. Without metallic nanoparticles, the reaction rate was found to be slow whereas the transportation of the charged species was accelerated in presence of the palladium nanoparticles.

From thermodynamics considerations, the above implies that the redox potential of the Pd-nanoparticles should be intermediate between the redox potential of the donor system, pyrrole-polypyrrole ( $D/D^+$ )  $E^0[D/D^+]$ , the lower threshold, and the redox potential of the acceptor system, 4NP and MB ( $A/A^-$ )  $E^0[A/A^-]$ , the upper threshold [62] (Scheme 3). The reaction between these systems, which is slow in the absence of the palladium, becomes efficient as a result of the electron transfer through the metal cluster relay. The Pd nanoparticles further lower the kinetic barrier, which facilitates a faster rate of reduction. If  $E^0[Pd^{2+}/Pd_{(nano)}]$  is higher than  $E^0[A/A^-]$ , as in a bulk metallic system, the electron is still transformed from D to  $Pd_{(bulk)}$ , but thermodynamics do not allow a relay effect to occur between  $Pd_{(bulk)}$  to A and, as a consequence, no catalytic effect has been observed [63]. Conversely, if the clusters are very small, the transfer of electrons is also not feasible due to the large potential difference. Thus, an effective transfer of electrons is only possible when the potential of the cluster is more positive than that of the electron donor system, i.e.,  $E^0[Pd^{2+}/Pd_{(nano)}] > E^0[D^+/D]$ . An effective relay of electrons is possible between an acceptor and a donor when ideal conditions are established, that is,  $E^0[A/A^-] < E^0[Pd^{2+}/Pd_{(nano)}] > E^0[D^+/D]$ .

The generally accepted mechanism of electron transport is due to successive hopping from molecule to molecule to overcome the trap caused by intra-molecular vibrations. In the

hopping mechanism, to evaluate the electron mobility, there are two rate processes at different spatial scales that have to be considered. The processes are the electron transfer within molecular dimers and the electron diffusion in organic solids or polymers. The first process can be characterized by an inter-molecular electron transfer at the atomistic level, while the latter can be simulated at the molecular level by the random walk technique [64]. In our first experiment in which APS was used as the oxidant, the electron transfer mechanism was through a strongly disordered system (polymer matrix) and is thus considered to be a short range electron transfer [65]. This is in contrast to the second experiment where the presence of palladium nanoparticles would enable the relay of electrons to follow a long-range hopping mechanism. The electron rich acceptor system accelerates the ‘proton hopping’ process through a Grotthuss mechanism and pulls the proton to the acceptor.

### Conclusions

In the present work, a metal-polymer composite material was designed using an *in-situ* polymerization and composite formation approach. Pyrrole and Pd-acetate were used as the precursor for the synthesis of a Pd-polypyrrole nanocomposite in which Pd-nanoparticles within the size range of 2-3 nm were highly dispersed and stabilized in the polypyrrole matrix. The Pd-polypyrrole composite material was used as an electrocatalyst for the electrochemical determination of tryptophan, a biomolecule and the precursor of different neurotransmitters. During the synthesis, Pd nanoparticles acted as a catalyst for the reduction of 4-nitro phenol, a model reaction being an example of a proton coupled electron transfer mechanism.

### Acknowledgements

The authors acknowledge financial support from the Research Committee and the Faculty of Science of the University of Johannesburg. One of us (MJW) gratefully thanks the Department of Science and Technology (DST), and the National Research Foundation (NRF) of South Africa for financial support. We gratefully acknowledge the constructive comments for the substantial improvement of the manuscript by one of the referees.

## References

- [1] C. J. Murphy, T. K. Sau, A. M. Gole, C. J. Orendorff, J. Gao, L. Gou, S. E. Hunyadi and T. Li, *J. Phys. Chem. B*, 2005, **109**, 13857.
- [2] S. H. Ko, I. Park, H. Pan, C. P. Grigoropoulos, A. P. Pisano, C. K. Luscombe and J. M. J. Fréchet, *Nano Lett.*, 2007, **7**, 1869.
- [3] K. Saha, S. S. Agasti, C. Kim, X. Li and V. M. Rotello, *Chem. Rev.* 2012, **112**, 2739.
- [4] E. C. Dreaden, A. M. Alkilany, X. Huang, C. J. Murphy and M. A. El-Sayed, *Chem. Soc. Rev.*, 2012, **41**, 2740.
- [5] M. Stratakis and H. Garcia, *Chem. Rev.*, 2012, **112**, 4469.
- [6] S. Scalzullo, K. Mondal, M. Witcomb, A. Deshmukh, M. Scurrrell and K. Mallick, *Nanotechnology*, 2008, **19**, 075708.
- [7] R. Narayanan and M. A. El-Sayed, *J. Am. Chem. Soc.*, 2003, **125**, 8340.
- [8] S.-W. Kim, M. Kim, W. Y. Lee and T. Hyeon, *J. Am. Chem. Soc.*, 2002, **124**, 7642.
- [9] E. Negishi, *Handbook of Organo-Palladium Chemistry for Organic Synthesis*, Wiley, Chichester, UK, 2002.
- [10] J. Tsuji, *Palladium Reagents and Catalysts*, Wiley, Chichester, UK, 2004.
- [11] K. Esumi, R. Isono and T. Yoshimura, *Langmuir*, 2004, **20**, 237.
- [12] N. Toshima and Y. Wang, *Adv. Mater.*, 1994, **6**, 245.
- [13] A. J. Bard, *Science*, 1980, **207**, 139.
- [14] I. Willner, R. Maidan, D. Mandler, H. Dürr, G. Dörr and K. Zengerle, *J. Am. Chem. Soc.*, 1987, **109**, 6080.
- [15] R. U. Islam, M. J. Witcomb, E. van der Lingen, M. S. Scurrrell, W. Van Otterlo and K. Mallick, *J. Organomet. Chem.*, 2011, **696**, 2206.
- [16] J. C. Martin, R. M. Wartell and D. C. O'Shea, *Proc. Natl. Acad. Sci.*, 1978, **75**, 5483.
- [17] M. J. L. Santos, A. G. Brolo and E. M. Girotto, *Electrochim. Acta*, 2007, **52**, 6141.
- [18] I. Rodríguez, B. R. Scharifker, J. Mostany, *J. Electroanal. Chem.*, 2000, **491**, 117.
- [19] A. Schmid, L. R. Sutton, S. P. Armes, P. S. Bain and G. Manfré, *Soft Matter*, 2009, **5**, 407.
- [20] T. W. Lewis, PhD thesis, Department of Chemistry, University of Wollongong, Australia, 1998. <http://ro.uow.edu.au/thesis/1107>.
- [21] L. Bansal and M. A. El-Sherif, *Intl. J. Smart Sensing and Intelligent Systems* 2010, **3**, 230.

- [22] L. J. Bellamy, *The Infrared Spectra of Complex Molecules*, Chapman & Hall, London, UK, 1980.
- [23] A. R. Fiorucci and E.T.G. Cavaleiro, *J. Pharm. Biomed. Anal.*, 2002, **28**, 909.
- [24] C. Li, Y. Ya and G. Zhan, *Colloids Surf. B*, 2010, **76**, 340.
- [25] X. Liu, L. Luo, Y. Ding and D. Ye, *Bioelectrochemistry*, 2011, **82**, 38.
- [26] K. A. Frith and J. L. Limson, *Electrochim. Acta* 2010, **55**, 4281.
- [27] G. Jin and X. Lin, *Electrochem. Commun.*, 2004, **6**, 454.
- [28] B. Fang, Y. Wei, M. Li, G. Wang and W. Zhang, *Talanta* 2007, **72**, 1302.
- [29] J. -B. Raoof, R. Ojani and H. Karimi-Maleh, *Electroanal.*, 2008, **20**, 1259.
- [30] S. Shahrokhian and L. Fotouhi, *Sensor. Actuat. B-Chem*, 2007, **123**, 942.
- [31] K. W. Park, J. H. Choi, B. K. Kwon, S. A. Lee and Y. E. Sung, H. Y. Ya, S. A. Hong, H. Kim, A. Wieckowski, *J. Phys. Chem. B*, 2002, **106**, 1869.
- [32] M. S. El-Deab and T. Ohsaka, *Electrochem. Commun.*, 2002, **4**, 288.
- [33] G. P. Jin, X. Peng and Q. Z. Chen, *Electroanal.*, 2008, **20**, 907.
- [34] S. Hrapovic, Y. Liu, K. B. Male and J. H. T. Luong, *Anal. Chem.*, 2004, **76**, 1083.
- [35] C. Y. Liu and J. M. Hu, *Biosens. Bioelectron.*, 2009, **24**, 2149.
- [36] Z. Li, X. Wang, G. Wen, S. Shuang, C. Dong, M. C. Paaou and M. M. F. Choi, *Biosens. Bioelectron.*, 2011, **26**, 4619.
- [37] A. P. Baioni, M. Vidotti, P. A. Fiorito and S. I. Córdoba de Torresi, *J. Electroanal. Chem.*, 2008, **622**, 219.
- [38] A. Salimi, R. Hallaj and S. Soltanian, *Electroanal.*, 2009, **21**, 2693.
- [39] P. Santhosh, K. M. Manesh, S. Uthayakumar, S. Komathi, A.I. Gopalan, K. P. Lee, *Bioelectrochem.* 75 (2009) 61.
- [40] T. V. Vernitskaya and O. N. Efimov, *Russ. Chem. Rev.* 1997, **66**, 443.
- [41] X. Zhang, J. Zhang, W. Song and Z. Liu, *J. Phys. Chem. B*, 2006, **110**, 1158.
- [42] A. Pron, Z. Kucharski, C. Budrowski, M. Zagorska, S. Krichene, J. Suwalski, G. Dehe and S. Lefrant, *J. Chem. Phys.*, 1985, **83**, 5923.
- [43] S. Machida, S. Miyata and A. Techagumpuch, *Synth. Met.*, 1989, **31**, 311.
- [44] Y. A. Dubitsky, B. A. Zhubanov and G. G. Maresch, *Synth. Met.* 1991, **41**, 373.
- [45] E. T. Kang, K. G. Neoh, Y. K. Ong, K. L. Tan and B. T. G. Tan, *Macromolecules*, 1991, **24**, 2822.
- [46] K. Mallick, M. J. Witcomb and M. S. Scurrrell, *Eur. Phys. J. E*, 2006, **19**, 149.
- [47] G. Wilkinson, R. D. Gillard and J. A. Mccleverty, *Comprehensive Coordination Chemistry*, Pergamon Press, Oxford, U.K, 1987.

- [48] R. G. Compton, *Comprehensive Chemical Kinetics*, Elsevier, New York, USA, 1989, vol. 28.
- [49] M. Robert, *Energy Environ. Sci.*, 2012, **5**, 7695.
- [50] J. J. Concepcion, J. W. Jurss, M. K. Brennaman, P. G. Hoertz, A. O. T. Patrocinio, N. Y. M. Iha, J. L. Templeton and T. J. Meyer, *Acc. Chem. Res.*, 2009, **42**, 1954.
- [51] S. Canaguier, V. Fourmond, C. Perotto, J. Fize, J. Pécaut, M. Fontecave, M. J. Field and V. Artero, *Chem. Commun.*, 2013, **49**, 5004.
- [52] M. Okamura, M. Yoshida, R. Kuga, K. Sakai, M. Kondo and S. Masaoka, *Dalton Trans.*, 2012, **41**, 13081.
- [53] M. M. Roubelakis, D. K. Bediako, D. K. Dogutan and D. G. Nocera, *Energy Environ. Sci.*, 2012, **5**, 7737.
- [54] C. Costentin, M. Robert and J. M. Savéant, *Phys. Chem. Chem. Phys.*, 2010, **12**, 11179.
- [55] S. Ohzu, T. Ishizuka, Y. Hirai, H. Jiang, M. Sakaguchi, T. Ogura, S. Fukuzumi and T. Kojima, *Chem. Sci.*, 2012, **3**, 3421.
- [56] K. Mallick, M. J. Witcomb, A. Dinsmore and M. S. Scurrall, *J. Mater. Sci.*, 2006, **41**, 1733.
- [57] D. N. Huyen, N. T. Tung, T. D. Vinh and N. D. Thien, *Sensors*, 2012, **12**, 7965.
- [58] A. G. MacDiarmid and A. J. Epstein, *Synth. Met.*, 1995, **69**, 85.
- [59] D. R. Weinberg, C. J. Gagliardi, J. F. Hull, C. F. Murphy, C. A. Kent, B. C. Westlake, A. Paul, D. H. Ess, D. G. McCafferty and T. J. Meyer, *Chem. Rev.*, 2012, **112**, 4016.
- [60] J. M. Mayer, D. A. Hrovat, J. L. Thomas and W. T. Borden, *J. Am. Chem. Soc.*, 2002, **124**, 11142.
- [61] A. Sirjoosingh and S. Hammes-Schiffer, *J. Phys. Chem. A*, 2011, **115**, 2367.
- [62] M. Mostafavi, J. L. Marignier, J. J. Amblard and J. Belloni, *Radiat. Phys. Chem.*, 1989, **34**, 605.
- [63] J. Belloni and M. Mostafavi, in: *Metal Clusters in Chemistry*, vol. III, eds., P. Braunstein, L.A. Oro and P.R. Raithby, J. Wiley, VCH, Germany, 1999, pp. 1213–1247.
- [64] Z. Shuai, L. Wang and C. Song, *Theory of Charge Transport in Carbon Electronic Materials, Springer Briefs in Molecular Science*, Springer, Berlin, Germany, 2012, pp. 7-41.
- [65] F. Liu, K. Khan, J. H. Liang, J. W. Yan, D. Y. Wu, B. W. Mao, P. S. Jensen, J. Zhang and J. Ulstrup, *ChemPhysChem*. 2013, **14**, 952.

## Figure captions

### Figure 1

SEM image (A) shows the chain-like morphology of the product (Pd–polypyrrole) with spherical units. The TEM image (B) shows the uneven surface on the spheres. Higher magnification TEM images (C and D) show the high density distribution of nanoparticles, within the range of 2–4 nm diameter, throughout the matrix.

### Figure 2

(A) EDX spectrum from the area shown in Fig. 1B. The palladium peaks are derived from the dark spots, whereas the copper peak comes from the TEM copper mesh support grid. (B) is the palladium 3d XPS spectrum, the peaks at binding energies at 335.35 eV for 3d<sub>5/2</sub> and 340.60 eV for 3d<sub>3/2</sub> are indicative of metallic palladium. XRD spectra (C), indicates the highly oriented, face-selective, crystalline character of the Pd-particles.

### Figure 3

In the Raman spectrum (A), the two sharp peaks at 1540 and 1589 cm<sup>-1</sup> are attributed to both the C=C ring stretching and the N–H in plane bending vibration of the Pd–polypyrrole composite material whereas in the FT-IR spectra, (B), the bands of the C–H and the N–H in-plane deformation vibration are located at 1021 cm<sup>-1</sup>. Spectrum (a) and (b) in (B) represent the FT-IR spectra of the Pd-polypyrrole and polypyrrole respectively.

### Figure 4

(A) is the cyclic voltammogram of (a) the bare GCE, (b) the polypyrrole modified GCE and (c) the Pd-polypyrrole modified GCE in 5.0 mM [Fe(CN)<sub>6</sub>]<sup>3-/4-</sup> (FCN) buffer solution at pH 7.5 maintaining a scan rate of 50 mV s<sup>-1</sup>. Cyclic voltammogram (B) is of (a) bare GCE and (c) polypyrrole modified GCE without analyte, while (b) is of the bare GCE and (d) is of the polypyrrole modified GCE in 0.2mM tryptophan containing PBS (Phosphate Buffered Saline), (0.01mM) buffer at a pH 7.5 and using a scan rate of 50 mV s<sup>-1</sup>.

### Figure 5

Cyclic voltammogram of Pd-polypyrrole modified GCE (a) in absence of tryptophan and with the increasing concentration of tryptophan (b) 0.20 mM, (c) 0.40 mM and (d) 0.60mM in 0.01mM PBS buffer solution at pH 7.5 at a scan rate of 50 mVs<sup>-1</sup>.

### Figure 6

(A) UV-vis spectra of the 4NP (10<sup>-4</sup> mol dm<sup>-3</sup>) in the presence of pyrrole (10<sup>-2</sup> mol dm<sup>-3</sup>) and APS (10<sup>-2</sup> mol dm<sup>-3</sup>) at different time intervals. Incomplete quenching of the absorbance peak (a) at 400 nm in the 4NP spectra took 204 min. The emergence of the peak at about 320 nm, peak (b), is due to the formation of the polymer. (B) (a) UV-vis spectrum of the 4NP and (b) the UV-vis spectrum of the 4NP in the presence of pyrrole (10<sup>-2</sup> mol dm<sup>-3</sup>) and K<sub>2</sub>PdCl<sub>4</sub>

( $10^{-2}$  mol dm $^{-3}$ ) after 2 min. The absorption band at 325 nm results from the  $\pi^*-\pi$  transition due to the formation of polypyrrole. A shoulder-like feature in the region of 375–450 nm corresponds to the bipolaron transition.

### Figure 7

(A) (a) UV-vis spectra of the MB ( $10^{-4}$  mol dm $^{-3}$ ) and (b) UV-vis spectra of the MB ( $10^{-4}$  mol dm $^{-3}$ ) in the presence of pyrrole ( $10^{-2}$  mol dm $^{-3}$ ) and APS ( $10^{-2}$  mol dm $^{-3}$ ). Incomplete quenching of the absorbance peak at 665 nm of the MB spectra took 60 min. (B) (a) is a UV-vis spectra of the MB ( $10^{-4}$  mol dm $^{-3}$ ) and (b) the UV-vis spectra of the MB ( $10^{-4}$  mol dm $^{-3}$ ) in the presence of pyrrole ( $10^{-2}$  mol dm $^{-3}$ ) and K $_2$ PdCl $_4$  ( $10^{-2}$  mol dm $^{-3}$ ). From (B), curve (c), the MB spectra can be seen to have disappeared after 5 mins due the addition of pyrrole and K $_2$ PdCl $_4$ .

### Figure 8

UV-vis spectra of (a) polypyrrole and (b) the Pd-polypyrrole composite. In both the spectra, the absorption band in the range of 300 to 350nm corresponds to the  $\pi^*-\pi$  transition resulting from the formation of polypyrrole. A shoulder-like appearance observed from 415 to 500 nm (indicated by an arrow, in spectrum (a)) corresponds to a bipolaron transition, a characteristic feature for the oxidized state of polypyrrole. A broad absorption band starting from 450 nm to around 750 nm in spectrum b, can be assigned to a bipolaron transition, which is a feature of the oxidized state of polypyrrole.

Figure: 1

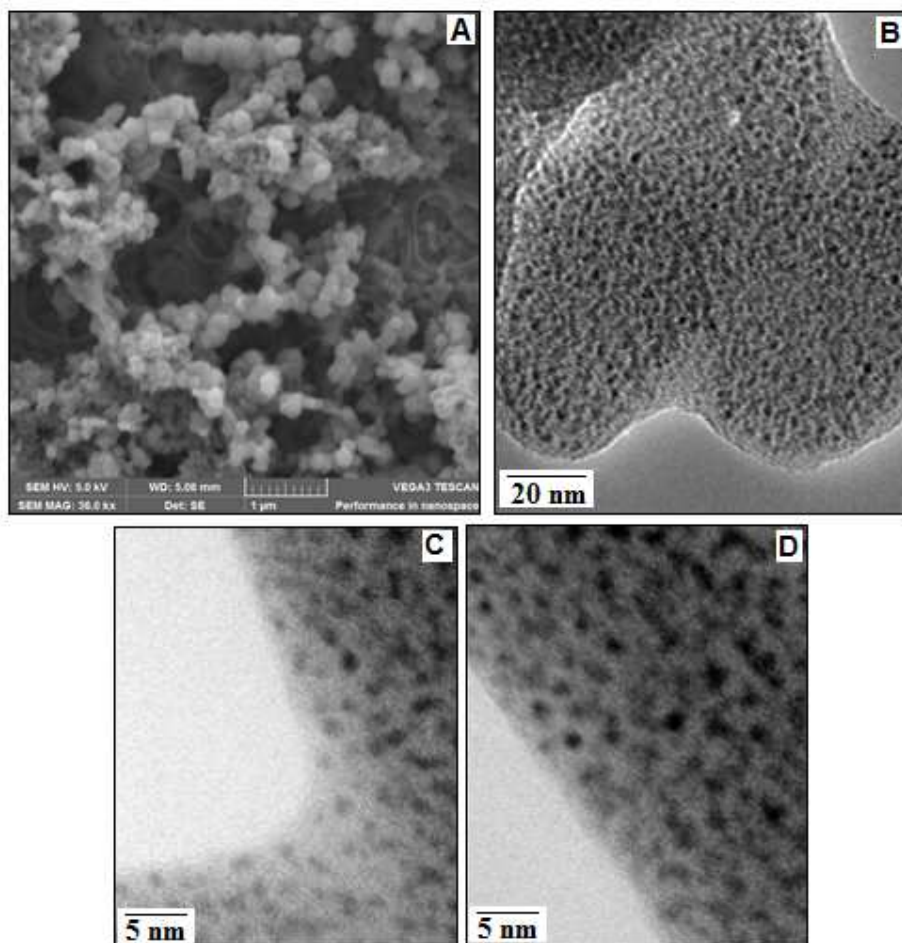


Figure: 2

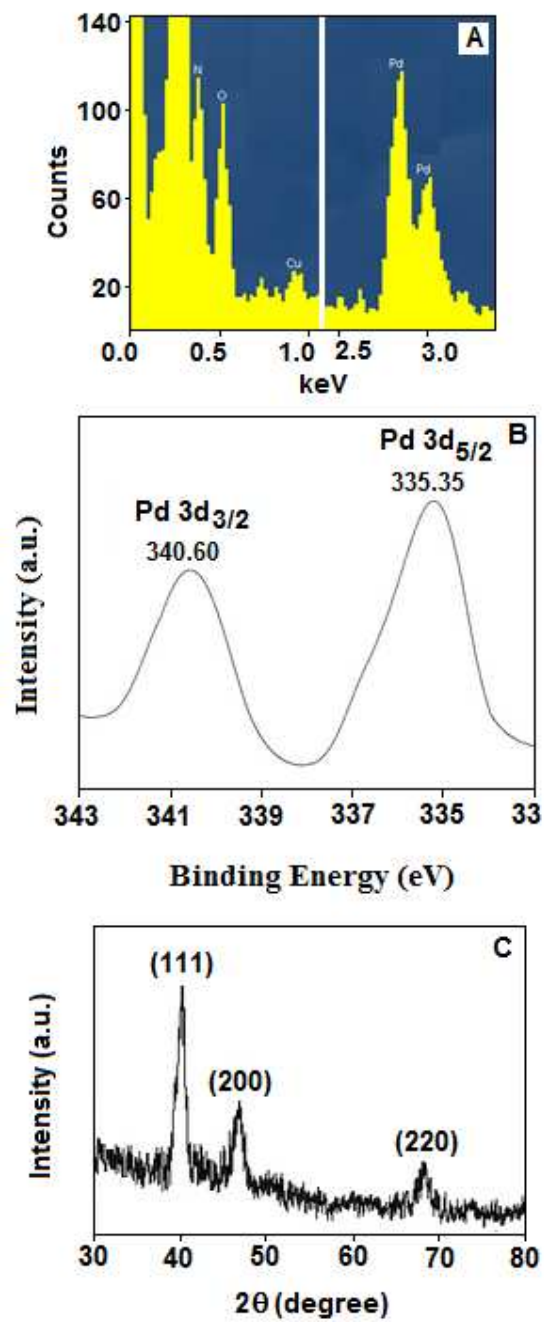


Figure: 3

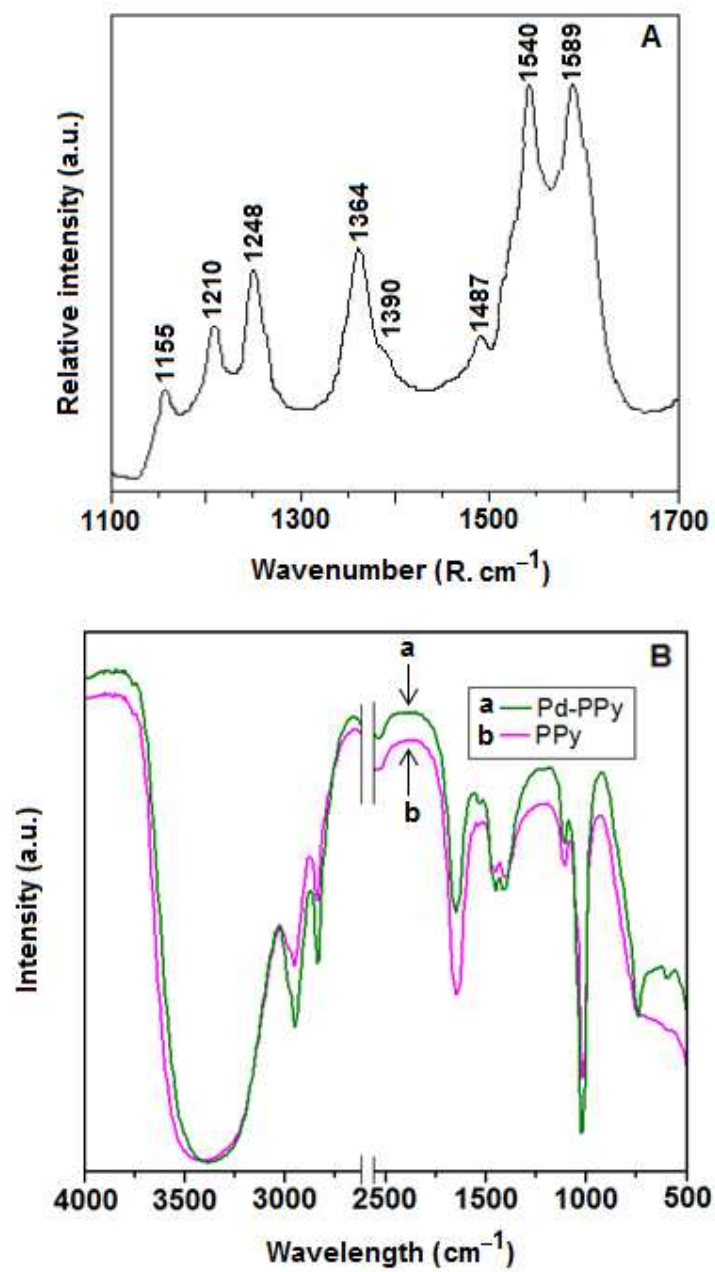


Figure: 4

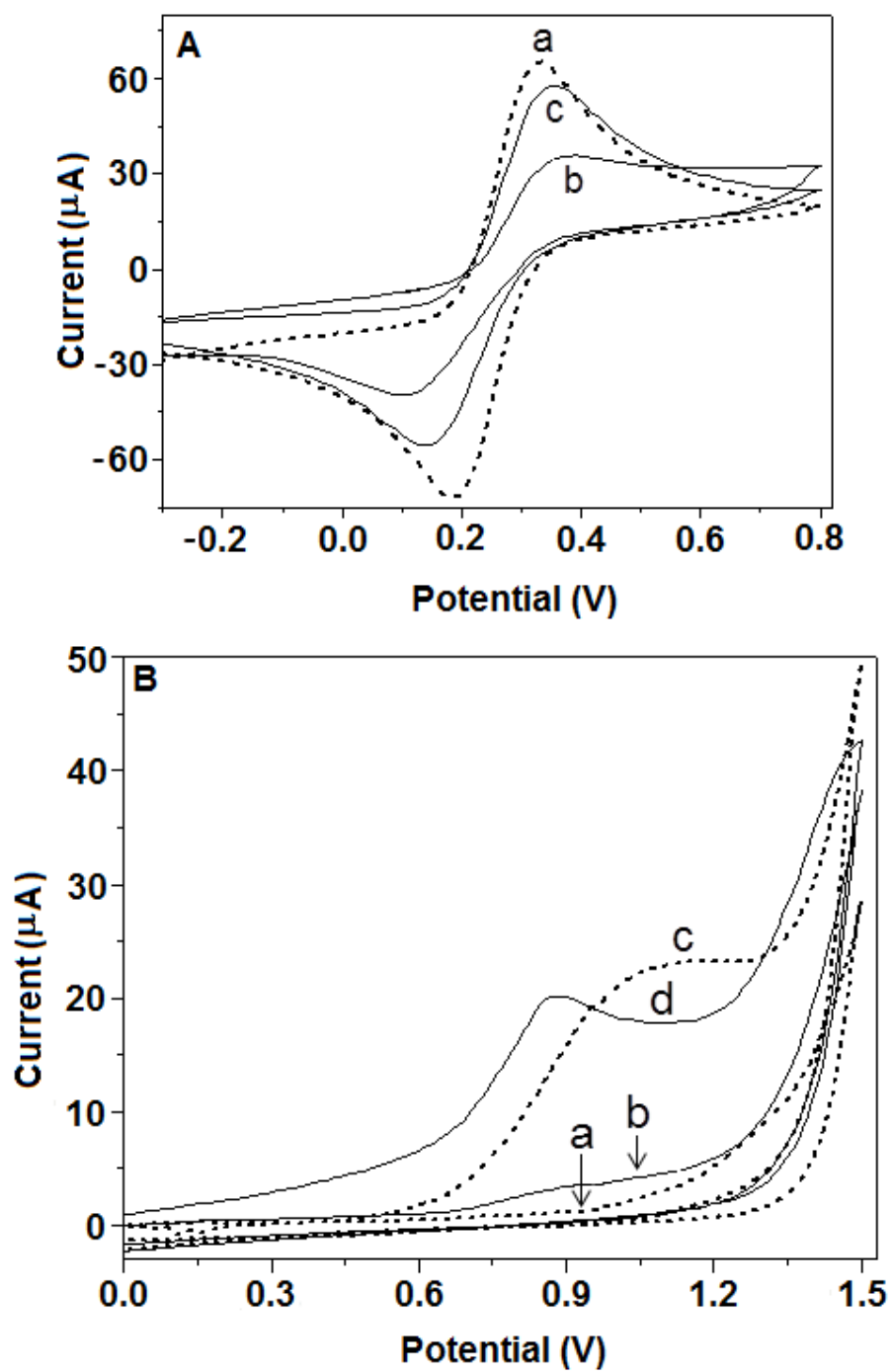


Figure: 5

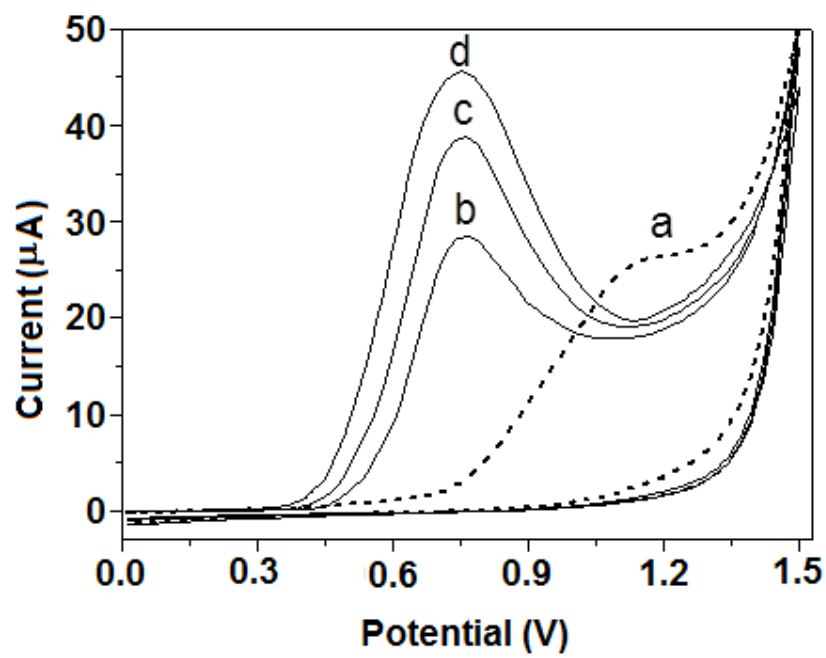


Figure: 6

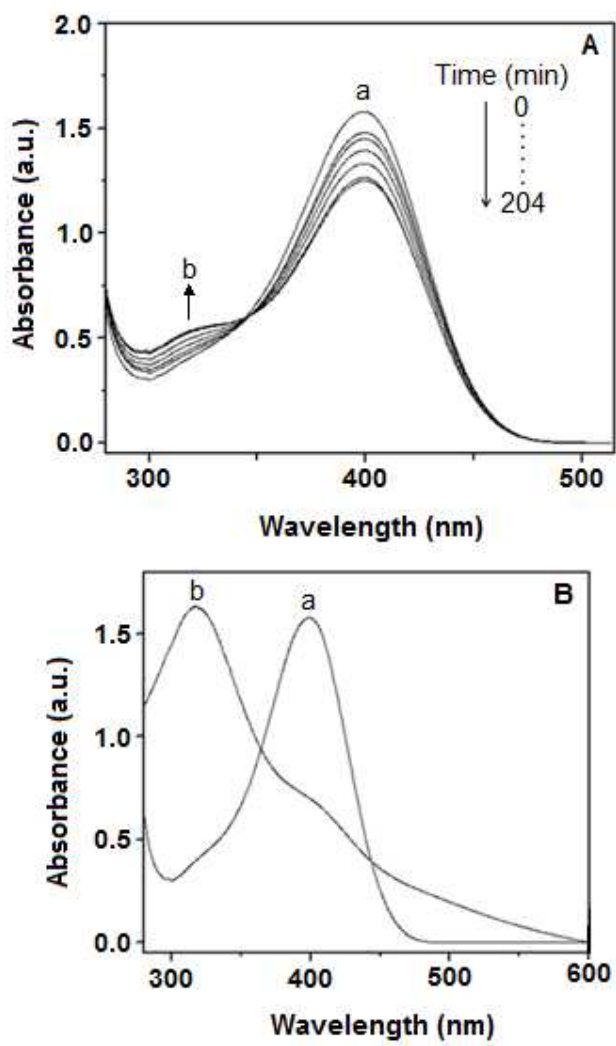


Figure: 7

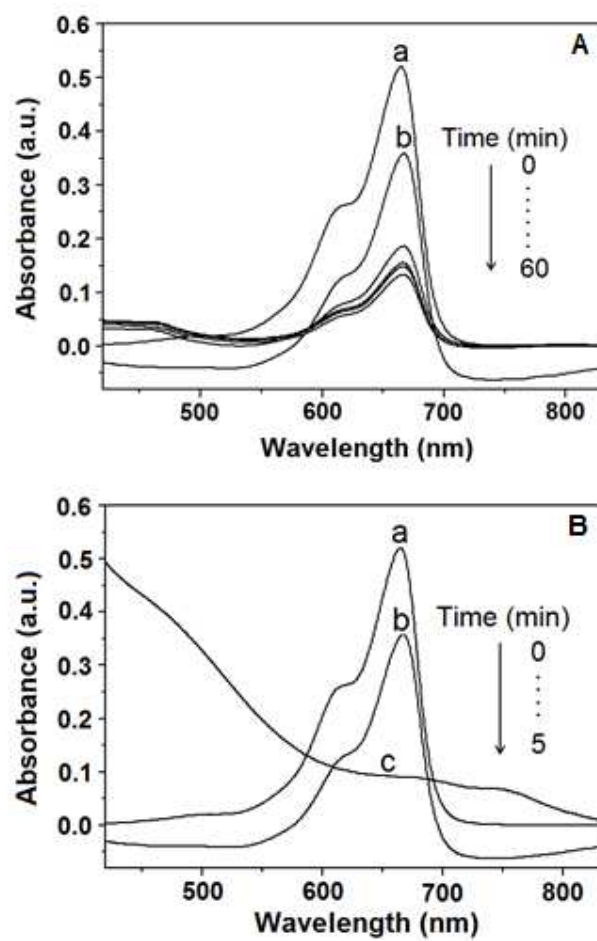
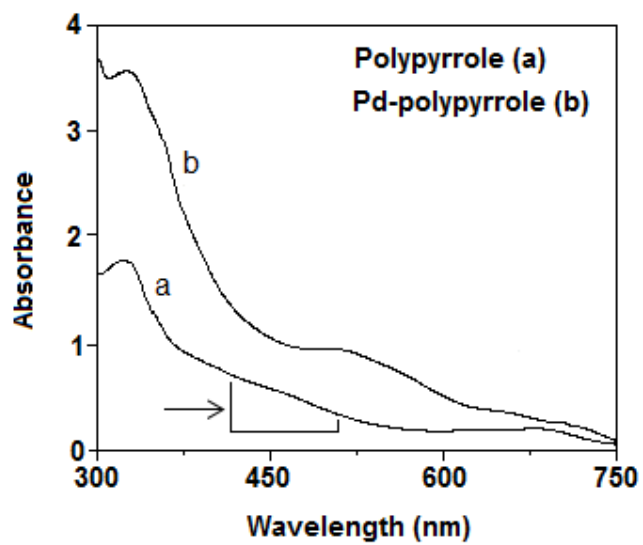


Figure: 8



## Scheme captions

**Scheme: 1**

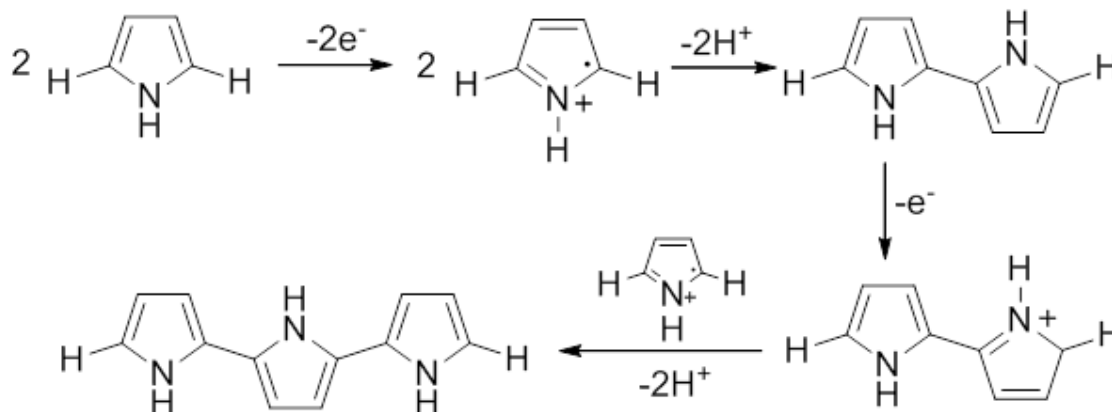
Oxidative polymerisation of pyrrole.

**Scheme: 2**

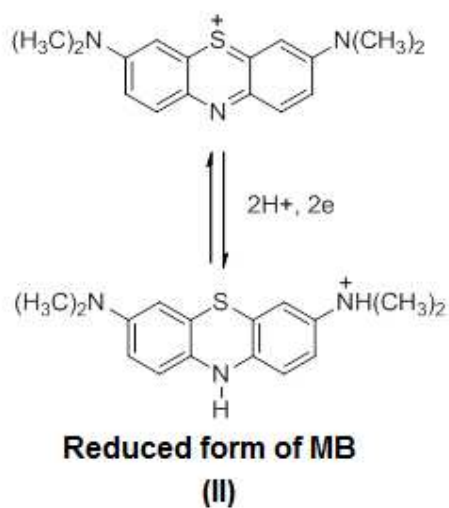
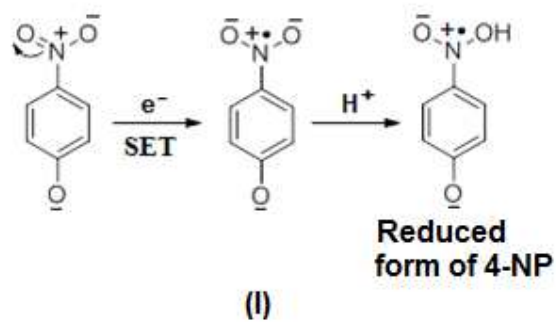
Proton coupled electron transfer mechanism for the reduction of 4NP and MB.

**Scheme: 3**

The mechanism of the catalytic electron transfer process. The metal cluster relays the electron from the donor molecule to the acceptor molecule. The schematic shows the thermodynamic conditions to be fulfilled when the cluster redox potential is higher than the donor (D) potential and lower than the acceptor (A) potential. A = dye in the oxidised form; A<sup>-</sup> = dye in the reduced form. D<sup>+</sup> = donor in the oxidised form; D = donor in the reduced form. E<sup>0</sup> is the redox potential.

**Scheme: 1**

Scheme: 2



Scheme: 3

